

Article

Convolvulus microphyllus Extract as a Green, Effective, and Affordable Corrosion Inhibitor: Theoretical Calculations and Experimental Studies

 Rajesh Haldhar ¹ , Ramkumar Vanaraj ¹, Omar Dagdag ^{2,*} , Avni Berisha ³  and Seong-Cheol Kim ^{1,*}
¹ School of Chemical Engineering, Yeungnam University, Gyeongsan 38541, Republic of Korea; rajeshhaldhar.lpu@gmail.com (R.H.); srirams27@gmail.com (R.V.)

² Centre for Materials Science, College of Science, Engineering and Technology, University of South Africa, Johannesburg 1710, South Africa

³ Department of Chemistry, Faculty of Natural and Mathematics Science, University of Prishtina, 10020 Prishtina, Kosovo; avni.berisha@uni-pr.edu

* Correspondence: omar.dagdag@uit.ac.ma (O.D.); sckim07@ynu.ac.kr (S.-C.K.)

Abstract: This study demonstrates the ability of *Convolvulus microphyllus* extract to prevent low-carbon steel corrosion (LCS) by varying inhibitor concentration. The effectiveness of the corrosion reaction was examined using gravimetric techniques and electrochemical procedures in a corrosive 0.5 M sulfuric acid medium. The results of polarization show a mixed adsorption nature on the LCS surface. *C. microphyllus*-derived film (extract) had an inhibition efficiency (IE) of 92.47% at an inhibitor concentration of 600 mg/L and a temperature 298 K. To examine the morphology, a scanning electron microscope (SEM) and atomic force microscope (AFM) were used to analyze the external films that protect LCS from sulfuric acid. A thin protective coat of inhibitor outside the LCS substrate follows the Langmuir adsorption isotherm. Additionally, computational exploration provided vital insights. The results of these experimental inhibitory outcomes are consistent with those of molecular dynamic simulations.

Keywords: *Convolvulus microphyllus*; natural corrosion inhibitor; surface morphology; electrochemical; theoretical calculations



Citation: Haldhar, R.; Vanaraj, R.; Dagdag, O.; Berisha, A.; Kim, S.-C. *Convolvulus microphyllus* Extract as a Green, Effective, and Affordable Corrosion Inhibitor: Theoretical Calculations and Experimental Studies. *Coatings* **2023**, *13*, 860. <https://doi.org/10.3390/coatings13050860>

Academic Editors: Hongwei Liu and Yongqiang Wang

Received: 13 April 2023

Revised: 28 April 2023

Accepted: 29 April 2023

Published: 30 April 2023



Copyright: © 2023 by the authors. Licensee MDPI, Basel, Switzerland. This article is an open access article distributed under the terms and conditions of the Creative Commons Attribution (CC BY) license (<https://creativecommons.org/licenses/by/4.0/>).

1. Introduction

Low carbon steel (LCS) is a basic metal that contains qualities from several different materials [1,2]. In addition to its use in acidic media and the consequent disintegration of low-carbon metals, it is now involved in numerous procedures such as cleaning, descaling, and pickling [3]. To cure or safeguard metals from environmental corrosion, inhibitors with phosphorus, oxygen, nitrogen, sulfur, and π -electronic frameworks are adsorbed on metal surfaces [4–7]. There are two methods for carrying out this adsorption: physisorption and chemisorption [8,9]. Physical adsorption happens at low temperatures and worsens as the temperature rises [10], and it has a lower activation energy. At normal temperatures, chemisorption occurs and worsens as the temperature rises [11,12]. In a natural process known as corrosion, metals start to corrode when they come into contact with moisture [13]. It is a combined development of hydrogen evolution and anodic corrosion of metals [14]. Another significant financial issue is this that metals must be shielded from corrosion. There are several techniques to prevent corrosion in metals, but the majority of them are both expensive and unfriendly to the environment [15]. Various agricultural materials are non-toxic, non-hazardous, and environmentally beneficial, such as organic goods, seeds, dried leaves, bark, and the peels of some fruits. These materials are experts in corrosion resistance and are more advantageous due to their simple accessibility and affordable price [16]. The corrosion inhibition action depends on the key components in the phytochemicals. The greater the number of heteroatoms and aromatic rings present in the major

phytochemicals, the higher the corrosion inhibition efficiency. The main advantage of using *C. microphyllus* aerial parts extract as a corrosion inhibitor over other reported inhibitors is the presence of key phytochemicals present in this plant extract. *C. microphyllus*-derived film (extract) contains two key phytochemicals, kaempferol and p-hydroxycinnamic acid, which contain many heteroatoms and aromatic structures and can efficiently inhibit the corrosion process. Moreover, the geometry of these key phytochemicals plays a vital role in inhibiting action, where the presence of a linear structure is more desirable to cover the entire surface of the LCS surface, leading to maximum adsorption and thus enhancing the anti-corrosion properties.

The aerial parts of *C. microphyllus*-derived film (extract) (eco-waste) are generally present in our surroundings. To dispose of this waste, burning is often the common practice, which may cause air pollution. In this study, we aimed to use this plant waste as a natural corrosion inhibitor for steel in acidic media. This makes the waste a significant component in a financially sustainable environment. Another aspect of our research is to use this plant waste as a valuable product with a low manufacturing cost. In this study, we utilized a biomass extract as a natural corrosion inhibitor with high inhibitory performance at a low inhibitor concentration. Although there are numerous corrosion-resistant materials available, a large portion of them utilize synthetic engineered items that are poisonous and harmful to the climate [17–20]. Therefore, it is important to develop harmless, eco-friendly corrosion inhibitors. *C. microphyllus* is a remarkable plant that belongs to the *Convolvaceae* family. The leaves are small, round, and nearly clipped, bearing 1–33 blossoms. Many these species have been featured in business shows known as shankpushpi and bindweed. These plants are found across the world, from India to the coast of West Africa. They may also be found in Rajasthan, which is in the northern region of India. The two main phytochemicals found in *C. microphyllus*-derived film (extract) are kaempferol and p-hydroxycinnamic acid [21].

Our research is innovative in that it seeks to replace synthetic corrosion inhibitors with natural ones. It is also novel and efficient in that it uses natural waste as a corrosion inhibitor. The advantages of using natural extract as a green inhibitor include the following: (1) natural goods are safe for both humans and the environment, and (2) natural goods create a usable substance out of waste materials at a low cost. Additionally, compared to similar studies, the film (extract) made from *C. microphyllus* offers greater surface adsorption and corrosion inhibition effectiveness at lower inhibitor concentrations.

The corrosion resistance capabilities of *C. microphyllus*-derived film (extract) have been detected in sulfuric acid corrosive conditions through weight loss estimations and electrochemical evaluations. Additionally, using SEM and AFM technologies, the adsorption of the green inhibitor on the LCS surface was investigated. FTIR spectroscopy revealed various functional groups in the plant extract, and the adsorption phenomena were confirmed by UV-visible spectroscopy. Additionally, computational analyses using methmolecular dynamics simulations and density functional theory were conducted to validate the results of the experiments.

2. Experimental

2.1. Materials and Methods

The aerial parts of the *C. microphyllus* plant were collected from Dehradun, Uttarakhand, India. All synthetic compounds were purchased from Sigma Aldrich Incorporation (St. Louis, MO, USA). The low-carbon steel was purchased from a local hardware store. The steel sheet was cut as per the requirements of the studies. The chemical composition of the low carbon specimen used was 0.08% (C), 0.12% (P), 0.039% (Si), 0.43% (Mn), 0.45% (Cr), 0.43% (Cu), 0.27% (Ni), and 97.83% (Fe) (weight %) [22]. Low carbon steel specimens measuring 1.00 cm × 1.00 cm × 0.03 cm were used for the weight loss studies [23–25]. For electrochemical studies, low carbon steel specimens measuring 1.00 cm × 1.00 cm × 8.00 cm were used, with only 1.00 cm² of the surface exposed to the electrolyte (the remainder was covered with epoxy) [26]. The low-carbon steel specimens were sequentially abraded with

220, 400, 600, 800, 1000, and 1200 grades of sandpaper, then dried, cleaned with acetone, and washed with distilled water before use. In order to create the electrolyte (0.5 M H₂SO₄), 99.999% sulfuric acid (mw 98.08) was employed. The pH of the corrosive solution was approximately 2.

2.2. Preparation of Plant Extract

The extraction process involved collecting *C. microphyllus* and verifying it with a botanist, Professor Bhatt from LPU, India. The raw plant materials were washed under tap water, cleaned, and then dried under natural conditions. After the drying process, it was crushed and converted into a powder. The extraction process was carried out using the Soxhlet apparatus by adding 400 g of *C. microphyllus* powder to 1000 mL of MeOH. The obtained materials were separated and concentrated [27], resulting in an extraction yield of approximately 20%. The extract was then stored in a vacuum desiccation under a controlled temperature for further corrosion inhibition studies. Figure 1 presents a schematic illustration of the plant extract preparation process. The pH of the pure plant extract was approximately 9.

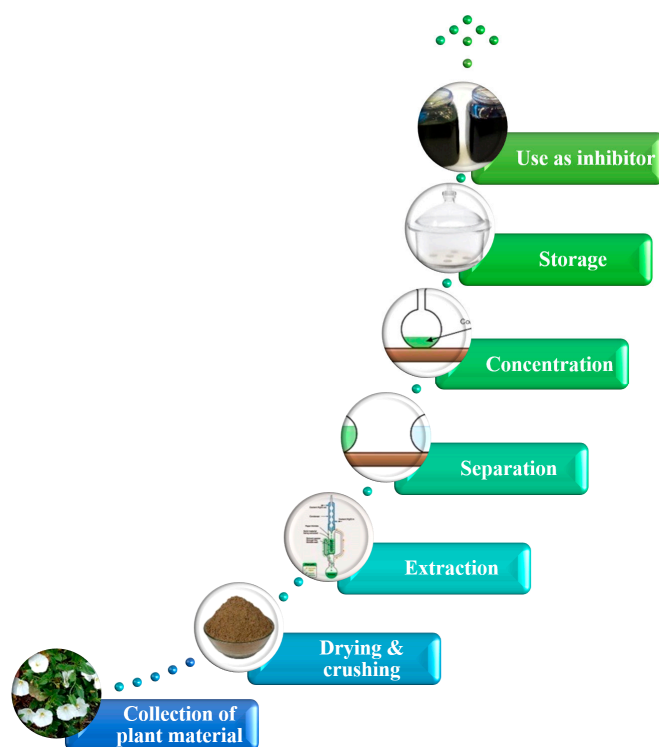


Figure 1. Schematic representation of the process of plant extract preparation.

3. Methods

3.1. Extract Characterization

3.1.1. FT-IR Analysis

In order to detect distinct active and aromatic groups, FT-IR data was employed. For the creation of a standard pallet, the plant extract and KBr were combined. Shimadzu's FTIR 8400S frequency spectrometer (Kyoto, Japan) was used to analyze this material over a range of 400 to 4000 cm⁻¹ [28].

3.1.2. UV-Visible Analysis

The test solution was examined using a Shimadzu UV-1800 UV-visible spectrophotometer before and after the corrosion test. The resultant spectrum was used to verify the procedure [28].

3.2. Weight Loss Study

The weight loss test was conducted in accordance with the American Society for Testing and Materials (ASTM) G 31-72. All the weight loss measurements took place between 298 K and 318 K over 24 h [29–31]. A water thermostat (PPI Fini X 48) was used to maintain the temperature throughout the process. For each experiment, 500 mL of newly made corrosive solution was utilized [32]. The metal sample was weighed for corrosion testing. The metallic samples were taken out of the test solution after the corrosion test (which lasted 24 h) and cleaned with distilled water as well as acetone, then dried with nitrogen flow. They were then weighed again to determine any weight loss [33]. All the weight measurements were made using Shimadzu electronic scales (BL-220H/D455006313).

3.3. Electrochemical Study

Potentiodynamic Polarization (PDP) measurements were performed after conducting electrochemical tests using electrochemical impedance spectroscopy (EIS) [34,35]. All electrochemical experiments were conducted using a CHI760E electrochemical workstation at 25 °C in 0.5 M sulfuric acid with varying inhibitor concentrations. A three-electrode model was used, which included a saturated calomel electrode (SCE) as the reference electrode, a platinum plate as the counter electrode, and a square of low carbon steel (1 cm²) as the working anode [36–39]. A freshly prepared electrolyte solution of 250 mL was used for all electrochemical tests [40]. The EIS curve was analyzed in the frequency range of 100,000 Hz to 0.01 Hz with an amplitude perturbation of 5.00 mV. When compared to the saturated calomel electrode, the Tafel curves were evaluated at a potential of ±250 mV and a scan rate of 1.00 mV s⁻¹ [41]. In the past, to acquire the Open Circuit Potential (OCP) constant, the working electrodes were submerged in the solution for 3600 s [42,43].

3.4. Surface Study

In addition to SEM and AFM analyses, this study employed a low-carbon steel model for an experiment on weight loss [44–46]. The metal samples were subjected to surface testing in an acidic environment with an inhibiting concentration of 600 mg/L. Studies on surface morphology provided evidence of the adsorption of inhibitor compounds on metal surfaces. The SEM and AFM models demonstrated the advantage of enhancing the surface adsorption of inhibitor molecules while producing a protective coating on the metal surface that shields it from an acidic environment [47]. The SEM experimental parameters, such as acceleration voltage, were set at 15 kV with a pressure of 20–10 Pa. The NT-MDT-INTEGRA set was designed for AFM, and the LEO-435 VP set was used for SEM microphotographs.

3.5. Computational Studies

3.5.1. DFT

Computational research has enabled a deeper comprehension of adsorption methods and confirmed the occurrence of this experiment. Here, quantum computation was employed in combination with theoretical tests. Plants are known to have multiple phytochemical components, and in this analysis, we selected the most important component in the plant *C. microphyllus* [21]. The selection of molecules or phytochemicals was achieved using quick handling Density Functional Theory (DFT) with a HyperChem software package using a DFT/B3LYP functional and 6-31G (d,p) basis set [48–50]. Crucial values were obtained from the optimized structures of examined inhibitor molecules.

3.5.2. MD Simulations

In order to ascertain the strength and nature of the molecular interactions on the surface of metallic Fe(110), a molecular dynamics simulation (MDS) was carried out [51,52]. The modeling was carried out using Material Studio, with a simulated grid size of 32.270 × 32.270 × 34.134 Å³. Periodic boundary conditions with composites (inhibitors, 20H₃O⁺ + 10SO₄²⁻ + 500H₂O) and Fe(110) were also used. The design was evaluated at 298 K with

an NVT simulation duration of 1000 ps and a time step of 1.0 fs under the direction of an Andersen thermostat [53].

3.6. Statistical Analysis

All experiments were performed in triplicate, and the results were presented according to the mean of different measurements \pm standard deviation. The statistical analysis was performed using the ANOVA method according to the Dunnett experiment with SPSS version 23 (SPSS Inc., Chicago, IL, USA), or the Kruskal-Wallis and Mann-Whitney test.

4. Results and Discussions

4.1. Characterization of *C. microphyllus* Extract

4.1.1. FT-IR Study

The FT-IR strategy was utilized to identify the presence of different functional groups and aromatic gatherings in the plant material. The FTIR spectra of the pure *C. microphyllus* plant extract are shown in Figure 2.

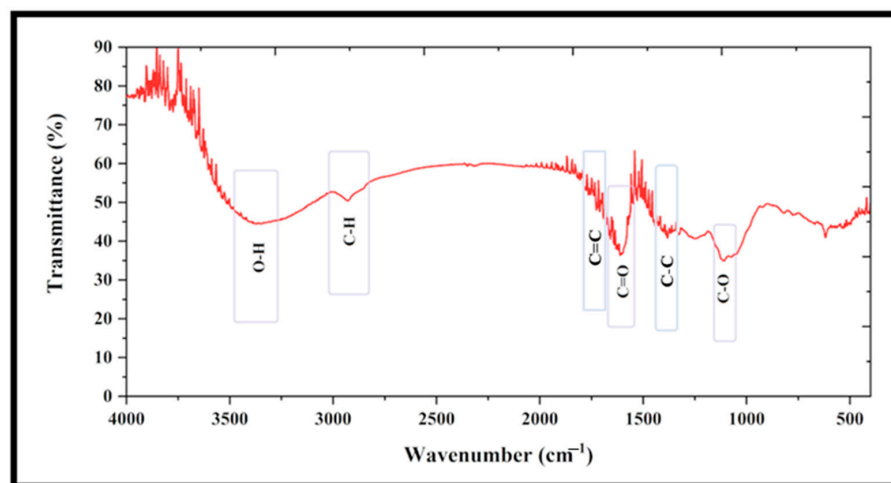


Figure 2. FTIR spectra of pure *C. microphyllus* plant extract.

The specific peaks found in *C. microphyllus* plant extract were related to the various functional groups that are listed in Table 1. In the pure *C. microphyllus* plant extract, the obtained spectra confirmed the presence of CH_2 (aromatic), C–O, –OH, and C = O groups, suggesting the availability of aromatic and heteroatoms in the sample [54]. These heteroatoms can easily transfer their electrons, which do not bind the vacant d-orbit to the LCS metal to form a compound. Aromatic molecules or parts can also use their electron segregation to aid in the surface adsorption of inhibitory molecules on the metal surface. As the plant extract is a complex organic mixture, it may contain many C–C and C=C bonds [55]. The small peaks near 1620 cm^{-1} to 1680 cm^{-1} were due to the presence of C=C bonds, while a few small peaks around 1200 cm^{-1} to 1400 cm^{-1} were due to the presence of C–C bonds [56].

Table 1. FT-IR spectra analysis of *C. microphyllus* extract.

FT-IR (Wavenumber; cm^{-1})	
2931.89	C–H stretching
1118.89	C–O stretching
1610.61	C=O stretching
3389.04	O–H stretching
1670.63	C=C stretching
1305.25	C–C stretching

4.1.2. UV-Visible Study

Further evaluation of the adsorption accuracy was done using UV-visible spectroscopy. The test was conducted both before and after the weight loss measurement. Figure 3 shows the UV-vis spectra of the inhibitory solution for both species.

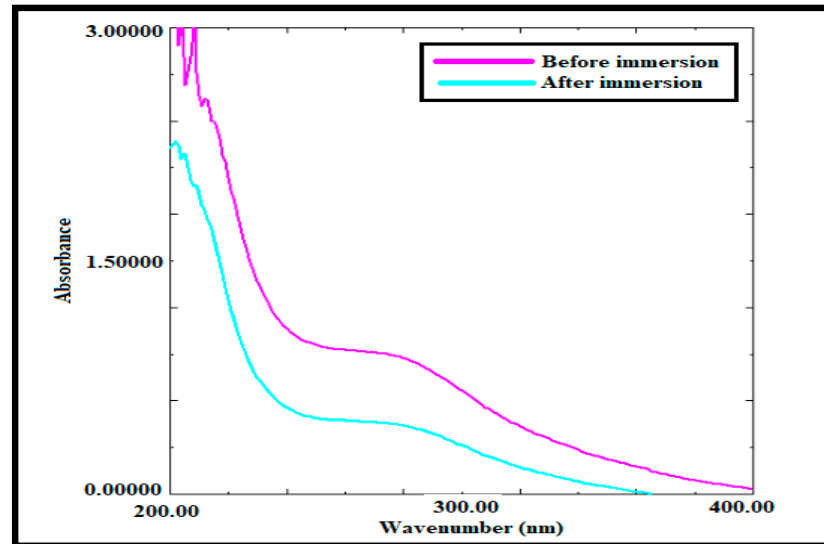


Figure 3. The inhibitor solution's UV-vis spectra in both modes.

The corrosion inhibitor solution exhibited two peaks at 218.00 nm as well as 287.00 nm prior to the weight loss examination, indicating $n-\pi^*$ and $\pi-\pi^*$ transitions, respectively [57]. The signal at 218.00 nm indicated a $\pi-\pi^*$ transition associated with the C=C conjugation of aromatic rings. A visible peak suggesting an $n-\pi^*$ transition of several functional groups, including heteroatoms such as oxygen, was detected in the frequency range of 250.00 to 350.00 nm. These results indicate that the adsorption peaks underwent a hypsochromic shift following the weight loss assessment [58,59]. The absorption maxima (λ_{max}) before immersion (218.00 nm 287.00 nm) shifted to a shorter wavelength (202.00 nm and 270.00 nm). The peak related to before immersion showed an absorbance maximum intensity of approximately 2.9 a.u. and 0.75 a.u., which decreased to approximately 2.65 a.u. and 0.65 a.u. after immersion. Additionally, the strength of the adsorption peaks was dramatically decreased. These modifications demonstrate that complex formation among inhibitor molecules and iron particles occurs at a certain point. When comparing the two spectra, it is generally agreed that the inhibitor molecules were able to detect an essential shift in the inhibitory adsorption particles' outer adsorption band.

4.2. Weight-Loss Study

A simple and manual testing procedure, the weight-loss approach provides insight into the link between inhibitor concentration and inhibition efficiency. This test was performed using the ASTM technique at 298 ± 0.5 K to 318 ± 0.5 K for 24 h with various inhibitor doses [14,53,60]. The following equations were used to obtain important parameters such as corrosion rate, inhibitory effectiveness, and surface coverage value [45]:

$$\Delta\omega = \omega_o - \omega_i \quad (1)$$

$$C_R = \frac{87,600 \times \Delta\omega}{AtD} \quad (2)$$

where:

C_R = corrosion rate ($\text{mm} \cdot \text{y}^{-1}$);

ω_o = initial weight of the LCS (g);

ω_i = final weight of the LCS (g);
 $\Delta\omega$ = weight loss of the LCS (g);
 $D = 7.86 \text{ g cm}^{-3}$ (density of iron);
 t = immersion time (h);
 A = area of the LCS (cm^2).

The following formulas were used to calculate the surface coverage values and the inhibitor's effectiveness [47]:

$$\text{IE}(\%) = \frac{\text{CorrosionRate} - \text{CorrosionRate}_{\text{inh}}}{\text{CorrosionRate}} \times 100 \quad (3)$$

$$\theta = \frac{\text{CorrosionRate} - \text{CorrosionRate}_{\text{inh}}}{\text{CorrosionRate}} \quad (4)$$

where:

θ = surface coverage values;
 $\text{CorrosionRate}_{\text{inh}}$ = corrosion rate of the LCS with inhibitor;
 CorrosionRate = corrosion rate of the LCS without inhibitor.

Table 2 displays the results of the weight loss tests, which indicate that as the inhibitor concentration increases, inhibition efficiency also increases, and the corrosion rate decreases [61]. The corrosion rate reaches up to 11.33 mmy^{-1} without the inhibitor, but at a concentration of 600 mg/L , the inhibitor exhibits the highest corrosion inhibition efficiency of 86.95% and reduces the corrosion rate to 1.47 mmy^{-1} . After 600 mg/L , no significant change was observed in inhibition efficacy, suggesting that 600 mg/L is the optimum or highest inhibitor concentration for achieving the best anti-corrosion performance. Based on these results, the Langmuir adsorption isotherm was also plotted [62]. In addition, we can observe that as the temperature increased, the corrosion inhibition performance of *C. microphyllus*-derived film (extract) decreased, which is attributed to the degradation of phytochemicals because phytochemicals are organic molecules that are known to easily degrade at higher temperatures.

Table 2. Corrosion rate and inhibition efficiency of *C. microphyllus*-derived film (extract) with different concentrations, both with and without inhibitor.

Temperature (K)	Inhibitor Concentration C (mg/L)	Corrosion Rate C_R (mmy^{-1})	Inhibition Efficiency IE (%)
298	Blank	11.33	-
	100	3.67	67.55
	200	3.08	72.74
	300	2.42	78.59
	400	1.89	83.27
	500	1.72	84.78
	600	1.47	86.95
308	Blank	15.29	-
	100	5.59	67.61
	200	4.70	72.81
	300	4.07	78.64
	400	3.51	83.31
	500	2.40	84.81
	600	2.39	87.02
318	Blank	19.14	-
	100	7.57	63.44
	200	6.33	69.26
	300	5.75	73.38
	400	4.91	77.04
	500	4.07	78.73
	600	3.88	79.73

4.3. Electrochemical Studies

4.3.1. OCP

Electrochemical experiments were conducted to assess the inhibitory power of the investigated plant extract and to determine the corrosion resistance of metals. The initial electrochemical test carried out was open circuit potential (OCP) measurements. Low-carbon steel samples were submerged in 0.5 M H₂SO₄ in both the absence and presence (600 mg/L) of the investigated inhibitor, and the corrosion potential was determined. Figure 4a shows a stable OCP both with and without an inhibitory concentration of 600 mg/L. When the potential rapidly drops after the first immersion, it usually indicates that the native oxide layer is dissolving. The creation of a protective coating on the surface is typically linked to the subsequent movement of the potential towards more positive values. In the EIS and PDP tests, low-carbon steel samples were immersed in the corrosive environment for one hour to ensure a stable open circuit potential. To describe the EIS diagram, we used a simple electronic equation model [63]. Measurement of the OCP took 200 s [14]. The low-carbon steel OCP was first reduced without inhibitors and then stabilized at 465 mVvs SCE. The stabilizer at 600 mg/L was stable at 463 mVvsSCE, which was due to the formation of an insoluble metal oxide layer on the metal surface. This indicates that there was a barrier molecule that changed the state of interaction between the carbon materials and electrolytes.

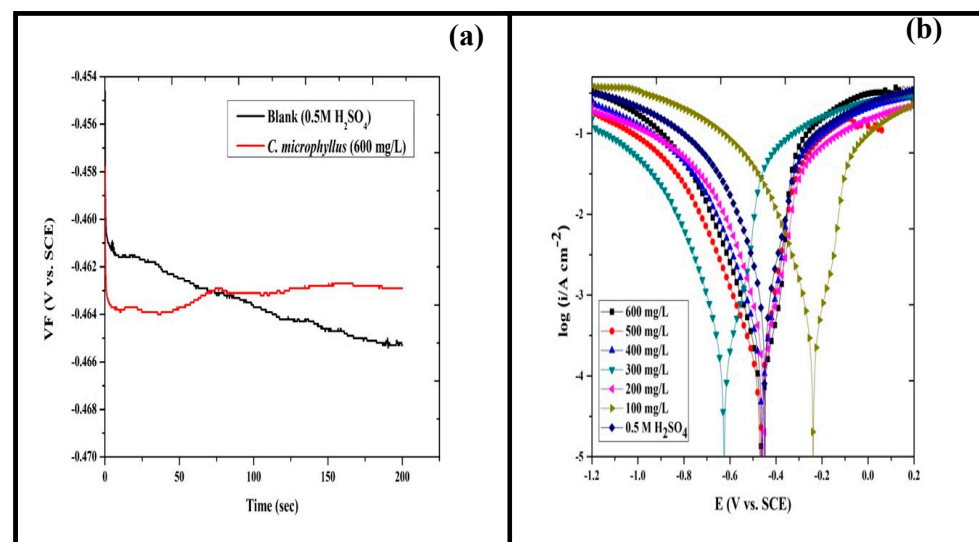


Figure 4. Stable OCP (a) and PDP curves (b) with and without several concentrations of inhibitor solution.

4.3.2. PDP

Polarization measurements in 0.5 M sulfuric acid made it possible to determine the corrosion resistance of low-carbon steel during adsorption. The polarization curve of low-carbon steel in the aggressive 0.5 M sulfuric acid environment at 298 K was observed with and without varying concentrations of *C. microphyllus*-derived film (extract), as shown in Figure 4b.

PDP measurements provide key parameters such as corrosion potential (E_{corr}), anodic tafel slope (β_a), cathodic tafel slope (β_c), and corrosion current density (i_{corr}). The corrosion resistance performance or corrosion inhibition efficiency was calculated using the following equation [64]:

$$\text{IE}(\%) = \frac{i_{\text{corr}} - i_{\text{corr}}^{\text{inh}}}{i_{\text{corr}}} \times 100 \quad (5)$$

where:

i_{corr} = the corrosion current density without inhibitor;
 $i_{\text{corr}}^{\text{inh}}$ = the corrosion current density with inhibitor.

The results of PDP for LCS both with and without *C. microphyllus*-derived film (extract) are shown in Table 3. The inhibitory-active chemicals in the *C. microphyllus* extract were adsorbed on the surface of the LCS and prevented corrosion of the metal in an acidic environment. The anodic as well as cathodic Tafel slopes became less steep as a result of this process [65]. The anodic Tafel slope (β_a) and cathodic Tafel slope (β_c) were altered with every increment of *C. microphyllus*-derived film (extract) concentration, demonstrating that the inhibitor molecules hinder the metal-dissolving process and the hydrogen evolution reaction. The observation that the cathodic and anodic Tafel slopes remained essentially unchanged before and after the addition of the *C. microphyllus* extract proves that charge transfer regulates the cathodic and anodic reaction processes. As a result, without altering the reaction mechanism, the main components of the *C. microphyllus* extract were adsorbed into the steel surface, preventing LCS corrosion. Several natural substances found in the *C. microphyllus* extract may electrostatically adsorb to the surface of steel and form strong coordination interactions with iron through their heteroatoms. The functional particles of the *C. microphyllus* extract are strongly bound to the steel surface due to the combination of physisorption and chemisorption. This protects the steel from corrosion, as evidenced by the decline in corrosion current density values. These results show that the corrosion current density decreases as the concentration of the *C. microphyllus* extract increases.

Table 3. PDP parameters of *C. microphyllus*-derived film (extract) for LCS in 0.5 M sulphuric acid.

C (mg/L)	$-E_{corr}$ (mV vs. SCE)	i_{corr} ($\mu\text{A cm}^{-2}$)	β_a (mV/dec)	$-\beta_c$ (mV/dec)	IE (%)
Blank	465	890.90	141.66	164.25	-
100	239	251.70	53.00	106.62	71.74
200	452	226.20	62.22	107.00	74.61
300	625	144.40	68.28	106.70	83.79
400	460	141.80	45.21	108.45	84.08
500	469	103.00	58.96	122.80	88.44
600	463	67.06	34.79	107.40	92.47

Additionally, it has been observed that as the concentration of *C. microphyllus*-derived film (extract) increases, the values of i_{corr} (corrosion current density) gradually decrease.

This might be due to the strong coordination link that exists between the free electrons of heteroatoms and the unoccupied d-orbitals of iron in the *C. microphyllus* extract [66]. The lowest i_{corr} value ($67.06 \mu\text{A cm}^{-2}$) was observed with the highest concentration of *C. microphyllus*-derived film (extract) at 600 mg/L concentration, resulting in an IE of 92.47%. Beyond 600 mg/L inhibitor concentration, there was no significant change observed in inhibition efficacy, indicating that 600 mg/L is the optimum or highest inhibitor concentration where it shows the best corrosion inhibition performance.

4.3.3. EIS

The EIS spectra were drawn using a Randle electric equivalent circuit. The Nyquist plots are shown in Figure 5a, and the Bode plots are shown in Figure 5b. The results are shown in Table 4. The following equations were used to determine the corrosion inhibition effectiveness and other important factors [67]:

$$IE(\%) = \frac{R_{ct}^{inh} - R_{ct}}{R_{ct}^{inh}} \times 100 \quad (6)$$

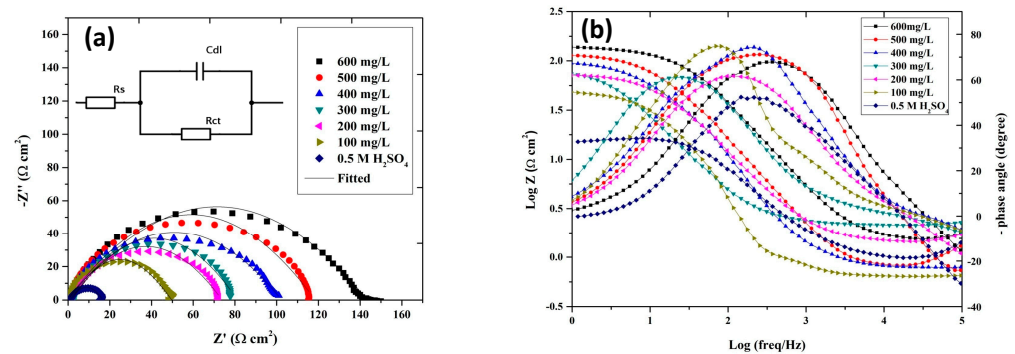


Figure 5. Nyquist curves (a) and Bode curves (b) for LCS with and without several concentrations of inhibitor solution (Z' = real, Z'' = imaginary, Z = vector of length, freq = Frequency).

Table 4. EIS parameters for *C. microphyllus*-derived film (extract) for LCS in 0.5 M sulphuric acid.

C (mg/L)	R_{ct} ($\Omega \text{ cm}^{-2}$)	C_{dl} ($\mu\text{F cm}^{-2}$)	IE (%)
Blank	15.71	269.00	-
100	49.98	247.43	68.56
200	72.58	232.19	78.35
300	76.40	220.21	79.43
400	104.60	211.34	84.98
500	117.09	205.05	86.58
600	155.13	155.15	89.87

The following equation was used to estimate the double-layer capacitance (C_{dl}) [68]:

$$C_{dl} = \gamma_0 (2\pi f_{\max})^{n-1} \quad (7)$$

where:

R_{ct}^{inh} = the charge transfer resistance with inhibitor;

R_{ct} = the charge transfer resistance without inhibitor;

γ_0 = the magnitude of the CPE;

f_{\max} = the frequency at maximum imaginary impedance;

$n = 2\alpha/\pi$;

α = the phase angle.

The corrosion of LCS is controlled by the charge transfer mechanism of corrosion, as represented by the capacitive loops. Figure 5a illustrates how the diameter of the semicircles grows as *C. microphyllus* extract is added to the corrosive media. The greater the corrosion inhibition, the larger the loop's diameter. In comparison to other concentrations, the *C. microphyllus*-derived film (extract) concentration at 600 mg/L exhibited the widest semicircle, indicating its superior corrosion resistance ability [69].

With increasing inhibitor concentration, C_{dl} decreased and R_{ct} increased, as shown in Table 4. The inductive loops associated with the EIS curves for the initial solution were at low frequencies due to the relaxation of the adsorbed product intermediates from the steel surface. Typically, the demise of the inductive loop is considered a "degradation" phenomenon for EIS for the remaining concentrations. The Nyquist plot's semicircle diameter variation trend was consistent with the impedance value variation trend in the Bode plot using *C. microphyllus* extract concentration in the Bode modulus curves. On all phase angle-frequency curves, a single wave could be observed, validating the Nyquist plot's one-time constant. In accordance with the literature, if the phase angle is equal to 90° or 0° , the electrochemical reaction at the steel solution interface is capacitive or resistive, respectively.

These findings demonstrate the remarkable surface adsorption of the film (extract) generated from *C. microphyllus*. The results of the EIS approach were consistent with

the PDP as well as measures of weight reduction. *C. microphyllus*-derived film (extract) exhibited 89.87% inhibition at 600 mg/L and R_{ct} ($155.13 \Omega \text{ cm}^2$). Beyond 600 mg/L inhibitor concentration, there was no significant change observed in inhibition efficacy, indicating that 600 mg/L is the optimum or highest inhibitor concentration for achieving the best corrosion inhibition performance.

4.4. Adsorption Isotherm

The Langmuir adsorption isotherm graph was created using data from trials on weight loss [70]. Figure 6 shows a graph of the Langmuir adsorption isotherm, which represents the relationship between the inhibitor concentration/surface coverage value and the inhibitor concentration (C/θ and C). Adsorption isotherms provide a clearer illustration of the interaction between the inhibitor molecules and the LCS surface. The ability of an inhibitor to inhibit corrosion depends on how efficiently its particle adsorbs to a metal surface. Reintroducing water particles to the metal solution interface is a step in the adsorption process. It was previously understood that the adsorption of natural inhibitor particulates between the metal and the solution is the first stage in reducing metal corrosion. Surface coverage is determined by the concentration of the inhibitor and the inhibition efficacy, expressed as ($\theta = \text{IE} (\%)/100$). With an increase in inhibitor concentration, more molecules are adsorbed onto the surface.

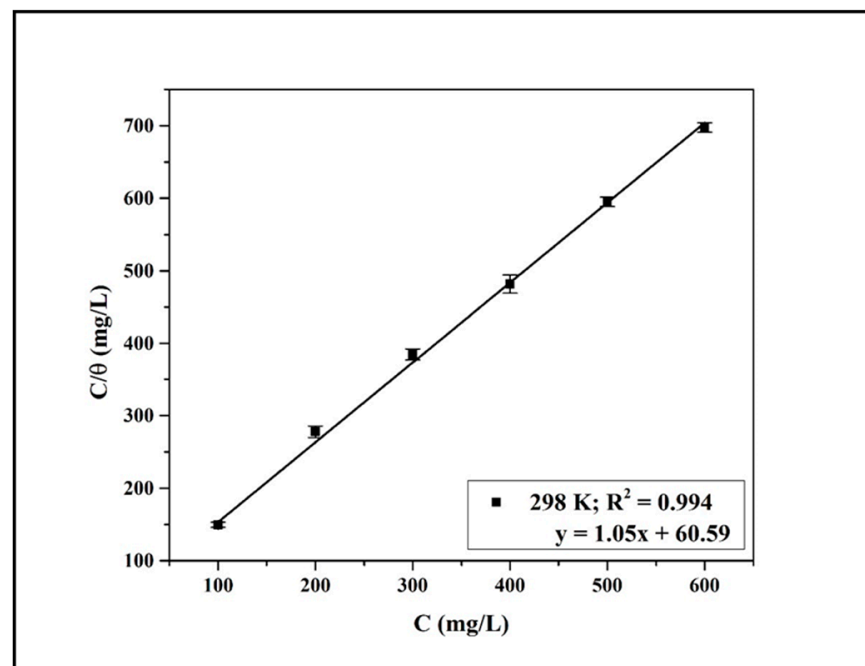


Figure 6. The Langmuir adsorption isotherm plot for *C. microphyllus* inhibitor.

It was previously stated that the inhibitor would follow Langmuir adsorption and form a monolayer on the metal surface if the regression coefficient and slope values were close to one. Our results indicate that the inhibitor follows the Langmuir isotherm and forms a protective monolayer over the metal surface to protect it from corrosive environments. The obtained values were extremely close to one. This occurrence can be described as [71]:

$$\frac{C}{\theta} = \frac{1}{K_{\text{ads}}} + C \quad (8)$$

where:

θ = the surface coverage;

C = inhibition concentration;

K_{ads} = the equilibrium adsorption constant.

4.5. Surface Studies

SEM and AFM Analysis

Using SEM and AFM methods, surface morphological investigations were conducted to obtain surface micrographs of LCS after the weight loss study with and without the inhibitor in the corrosive medium [72]. Figure 7 displays photomicrographs (SEM and AFM) of polished LCS surfaces following weight reduction with and without an inhibitor (600 mg/L). SEM and AFM photomicrographs of the used LCS surface before the test are shown in Figure 7a, which are referred to as polished LCS. The surface roughness was 2.99 nm, and the maximum height was 60 nm. SEM and AFM photomicrographs of the LCS surface during a weight loss test without an inhibitor are shown in Figure 7b [68]. The uneven SEM micrographs were apparent because of the high corrosion rate. The LCS surface was corroded, resulting in a severely corroded surface with a very high surface roughness value (138.81 nm) and a maximum height of 2100 nm. Figure 7c shows the LCS surface following the testing for weight loss with a 600 mg/L inhibitor concentration. This demonstrates that the inhibitor forms a shield on the LCS surface, shielding it from the corrosive medium and giving it a surface that is relatively smooth with a reduced surface roughness value (15.25 nm) and a maximum height of 160 nm [73]. The surface roughness values and maximum height values decreased from uninhibited to inhibited LCS. These lower values of surface roughness and maximum height for the inhibited LCS compared to the corroded LCS suggest surface adsorption and the creation of a protective thin film on the metal surface to protect it from the corrosive media. This shows that *C. microphyllus*-derived film (extract) absorbs on the metal surface, creating a protective layer to prevent corrosion on LCS surfaces.

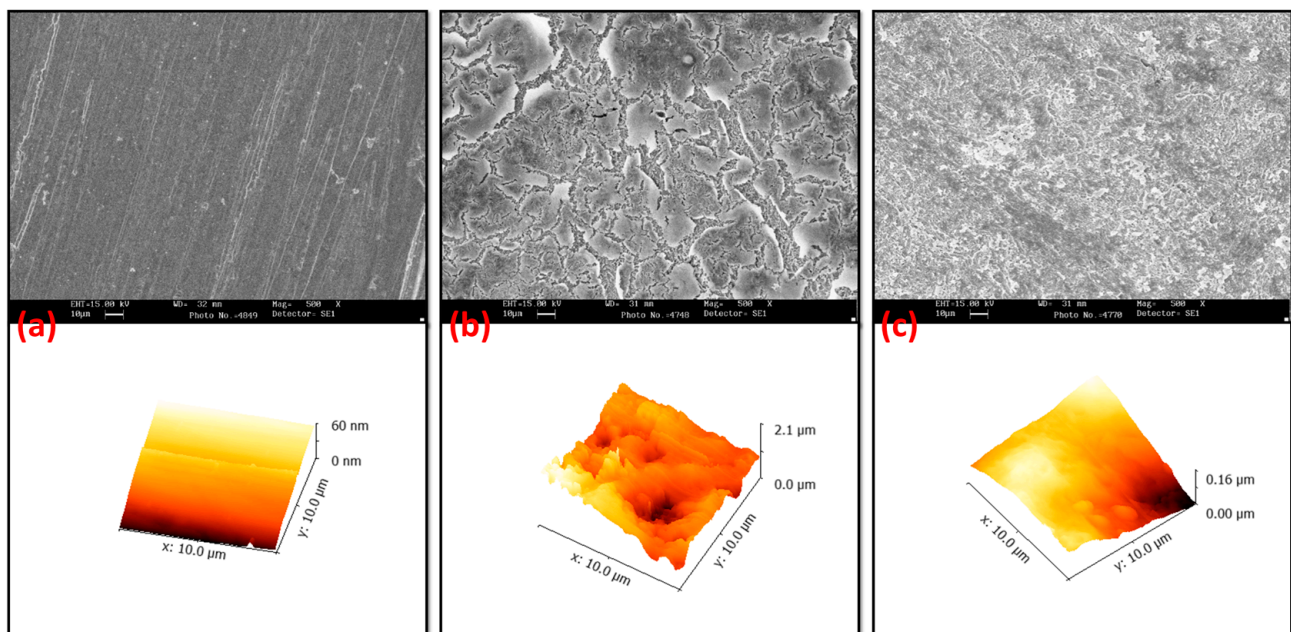


Figure 7. SEM and AFM micrographs of (a) polished, (b) corroded, and (c) protected surfaces of LCS. Reprinted with permission from [68]. Copyright 2021, Elsevier.

4.6. Computational Studies

4.6.1. DFT

Density functional theory has been used in computational investigations [74]. As referenced before, *C. microphyllus*-derived film (extract) is rich in phytochemicals, making it very hard to predict the corrosion inhibition activity of any specific molecule present in the *C. microphyllus* extract. Therefore, we chose two key/major phytochemical constituents for the DFT studies: kaempferol (M1) and p-hydroxycinnamic acid (M2), which are present in *C. microphyllus*-derived film (extract) [21]. Figure 8 displays the HOMO, LUMO, and MEP

(Molecular Electrostatic Potential) directions of kaempferol (M1) and p-hydroxycinnamic acid (M2). The key parameters were calculated using the following equations [60]:

$$\Delta E = E_{\text{LUMO}} - E_{\text{HOMO}} \quad (9)$$

$$\chi = -\frac{1}{2}(E_{\text{LUMO}} + E_{\text{HOMO}}) \quad (10)$$

$$\eta = \frac{1}{2}(E_{\text{LUMO}} - E_{\text{HOMO}}) \quad (11)$$

$$\sigma = \frac{1}{\eta} \quad (12)$$

$$\Delta E_{\text{BackDonation}} = -\frac{\eta}{4} \quad (13)$$

$$\Delta N = \frac{\chi_{\text{Fe}} - \chi_{\text{inh}}}{2(\eta_{\text{Fe}} - \eta_{\text{inh}})} \quad (14)$$

$$\pi = -\chi \quad (15)$$

where:

χ_{inh} = the electronegativity of the inhibitor molecule;

η_{inh} = hardness of inhibitor molecule;

χ_{Fe} = the electronegativity of the iron;

η_{Fe} = hardness of the iron;

E_{HOMO} = energy of highest occupied molecular orbital;

E_{LUMO} = energy of lowest un-occupied molecular orbital;

ΔE = energy gap;

σ = global softness;

ΔN = energy from inhibitor to metals;

π = chemical potential.

The vital components of kaempferol (M1) and p-hydroxycinnamic acid (M2) are shown in Table 5, which are significant due to their influence on the electron bonding of the inhibitor molecule with the metal ions. A low E_{LUMO} suggests that the molecule under evaluation has a strong potential for absorbing electrons [75]. A high E_{HOMO} score implies that the molecule under examination has a high potential for free electron donation. A stable inhibitor-metal combination is indicated by a low ΔE value. The capacity of the tested inhibitor molecule to donate electrons is indicated by a low value of χ [76,77].

Table 5. Theoretical parameters of kaempferol (M1) and p-hydroxycinnamic acid (M2).

Molecule	E_{HOMO} (eV)	E_{LUMO} (eV)	ΔE (eV)	ΔN (eV)	$\Delta E_{\text{Back-Donation}}$ (eV)	η (eV)	σ (eV ⁻¹)	χ (eV)	π (eV)
Kaempferol (M1)	-5.36	-2.41	2.94	0.22	-0.36	1.47	0.67	3.88	-3.88
p-hydroxycinnamic acid (M2)	-5.70	-2.51	3.19	0.27	-0.39	1.59	0.62	4.11	-4.11

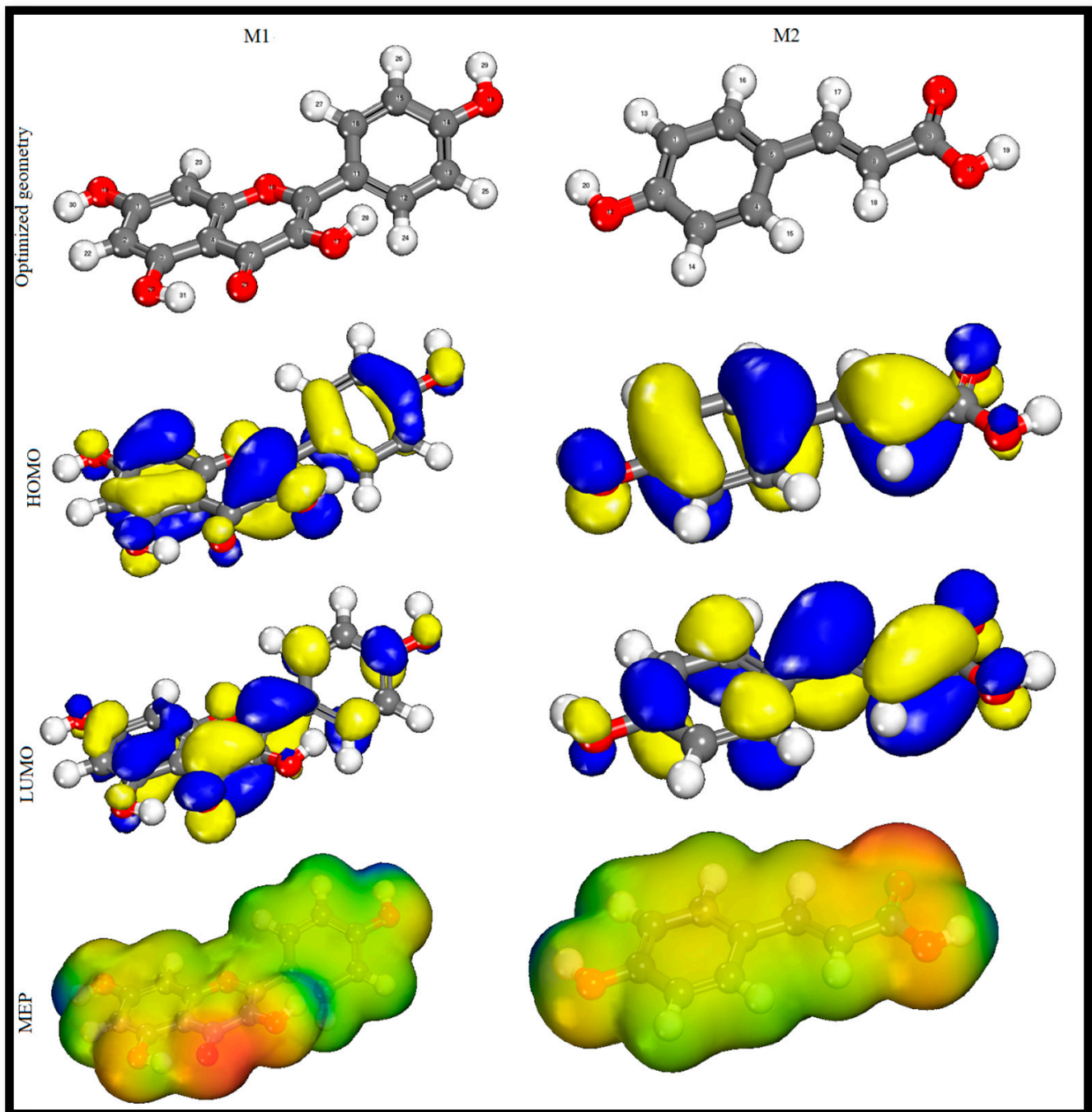


Figure 8. Optimized, HOMO, LUMO, and MEP structures of the M1 and M2 molecules.

4.6.2. MDS

The aim of this study was to theoretically or computationally investigate the influence of the test substances' adsorption on low carbon steel. Molecular dynamics simulations (MDS) were performed on the Fe(110) surface in a medium containing H_2SO_4 [78]. The optimal adsorption system for the inhibitor molecules (M1 and also M2) at the attack site is shown in Figure 9a. The investigated molecules (M1 and M2) were found to effectively adsorb at the molecular limit to reduce the density of the metal and the surface area of the corrosion cycle. Furthermore, surface and horizontal images showed how the *C. microphyllus* extract adhered to the surface of Fe(110), improving the performance of the film (extract) made from *C. microphyllus* on the primary iron layer.

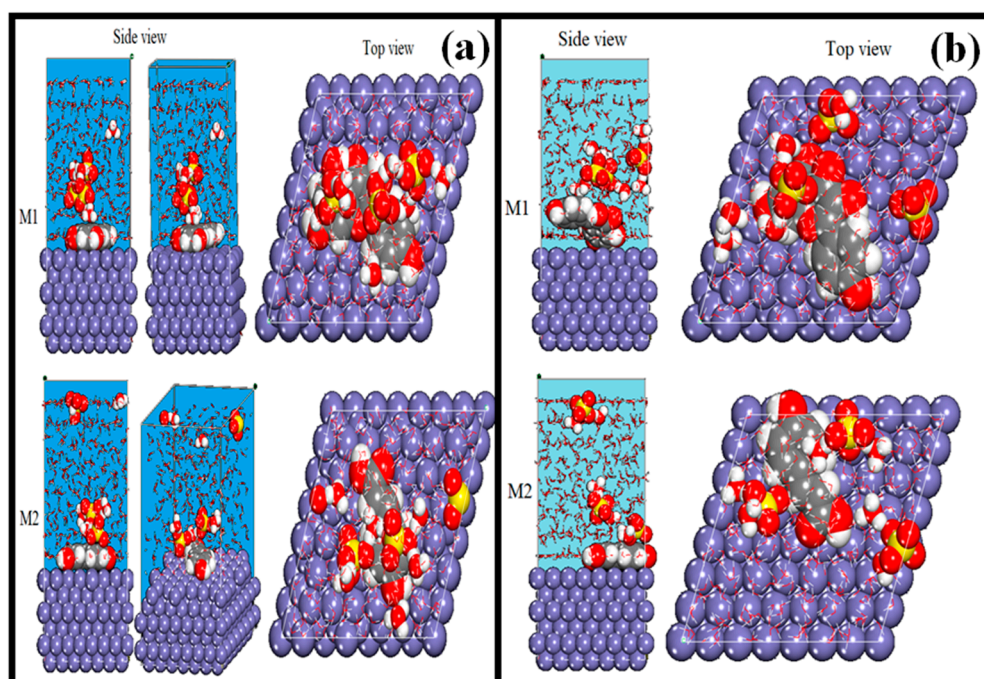


Figure 9. MDS (a) and MC (b) simulation of studied molecules on the metal (Fe(110)) surface.

The energies of adsorption and binding were used to compute the functions of chemical molecule adsorption and dissociation on the surface of the LCS. The binding energy (E_{binding}) and interaction energy ($E_{\text{interaction}}$) were calculated using the following equation [79]:

$$E_{\text{interaction}} = E_{\text{total}} - (E_{\text{surface+solution}} + E_{\text{inhibitor}}) \quad (16)$$

$$E_{\text{binding}} = -E_{\text{interaction}} \quad (17)$$

All the results are shown in Table 6. An inhibitor molecule's adsorption on the metal surface is indicated by a high binding value and a low interaction value, implying that *C. microphyllus*-derived film (extract) molecules are highly reactive with the LCS surface area [80].

Table 6. $E_{\text{interaction}}$ and E_{binding} energies of Kaempferol (M1) and p-hydroxycinnamic acid (M2).

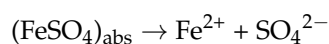
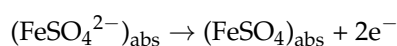
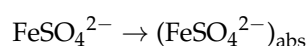
Systems	$E_{\text{interaction}}$ (kJ/mol)	E_{binding} (kJ/mol)
Fe(110)/M1	−620.00	620.00
Fe(110)/M2	−545.00	545.00

The findings demonstrate that p-hydroxycinnamic acid (M2) has a higher adsorption efficiency than kaempferol (M1) for subsequent uses. The outcomes of this experiment were validated using this system. The Monte Carlo simulation of the (Fe(110)-inhibitor) adsorption is depicted in Figure 9b. These findings imply that substances adhere to metal surfaces via coordination bonds [81].

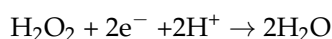
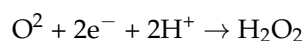
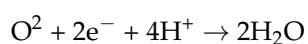
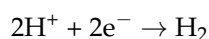
4.7. Inhibition Mechanism

To ensure the impact of *C. microphyllus*-derived film (extract) on the surface of low carbon steel in a corrosive environment containing 0.5 M sulfuric acid, the outcomes of this investigation need to be analyzed in terms of the electronic, chemical, and structural properties of inhibitory molecules. *C. microphyllus*-derived film (extract) contains different phytochemicals, which have various aromatic rings and heteroatoms [60]. As these molecules behave like a Lewis base, they establish coordination bonds with the free d-orbital of iron by donating their non-bonding electrons. They are then adsorbed onto the

metal surface. This procedure adds a protective coating to the metal substrate's surface to protect it from damage. Therefore, it is possible to anticipate that chemisorption and physisorption will affect the relationship between inhibitory particles and iron. The aromatic rings' π -electron content may be used for retro-donation [70]. Theoretical studies and polarization findings both support this conclusion. The structure of the kaempferol molecule for adsorption on a metal surface is shown in Figure 10. Figure 11 compares the relative corrosion inhibition efficiencies attained using weight loss, PDP, and EIS for various factors. Table 7 compares the effectiveness of previously published work with the current study in terms of inhibition. Li et al. [82] studied the suppression of copper in alkaline electrolytes using M@0.33P. The M@0.33P nanohybrids protection mechanism is explained by the corrosion inhibition mechanism, which points to a superior barrier effect and the interfacial passivation-maintenance process. Dong et al. [83] hypothesized that the corrosion attack sequence on the $\text{TiO}_2(110)$ surface was $\text{S}^{2-} > \text{CO}_3^{2-} > \text{Cl}^- > \text{HS}^- > \text{HCO}_3^-$ when corrosive ions (Cl^- , HS^- , S^{2-} , HCO_3^- , and CO_3^{2-}) adsorbed on the surface. The environment containing H_2S will cause substantial corrosion in TC4 titanium alloy, followed by the environment containing CO_2 , which has comparatively strong corrosion resistance to Cl^- . The corrosion of the TC4 titanium alloy will be more severe when the corrosion products H_2S , CO_2 , and Cl^- coexist in the corrosion medium. Liu et al. [84] investigated supermolecular assemblies based on benzothiazole derivatives as effective copper corrosion inhibitors in artificial seawater. Following a cathodic-dominated mixed-type inhibition mechanism, the authors hypothesized that MBT and ABT were stably integrated into β -CD with differing thermodynamic characteristics, yielding optimum inhibition efficiencies of 95.6% and 89.2% at a 0.5 g/L dose. The corrosion inhibition of metal involves two reactions (anodic and cathodic reactions). The anodic reaction mechanism of iron in sulfuric acid solution takes place in two continuous steps:



The cathodic reaction is as follows:



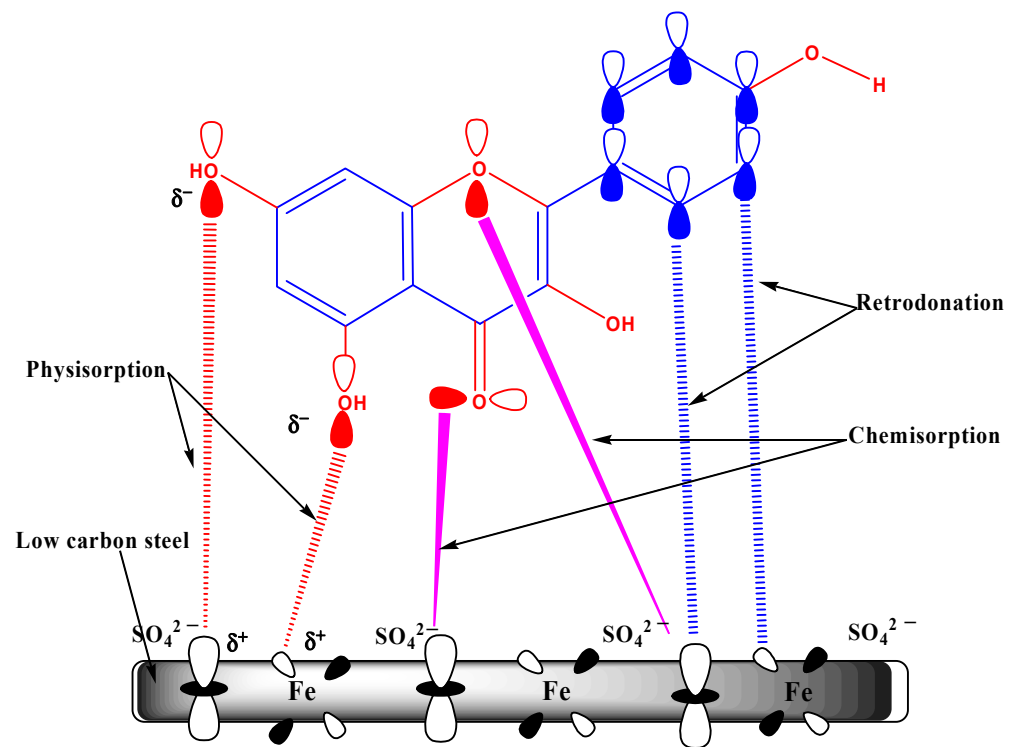


Figure 10. Proposed adsorption phenomenon of kaempferol molecules on the LSC surface.

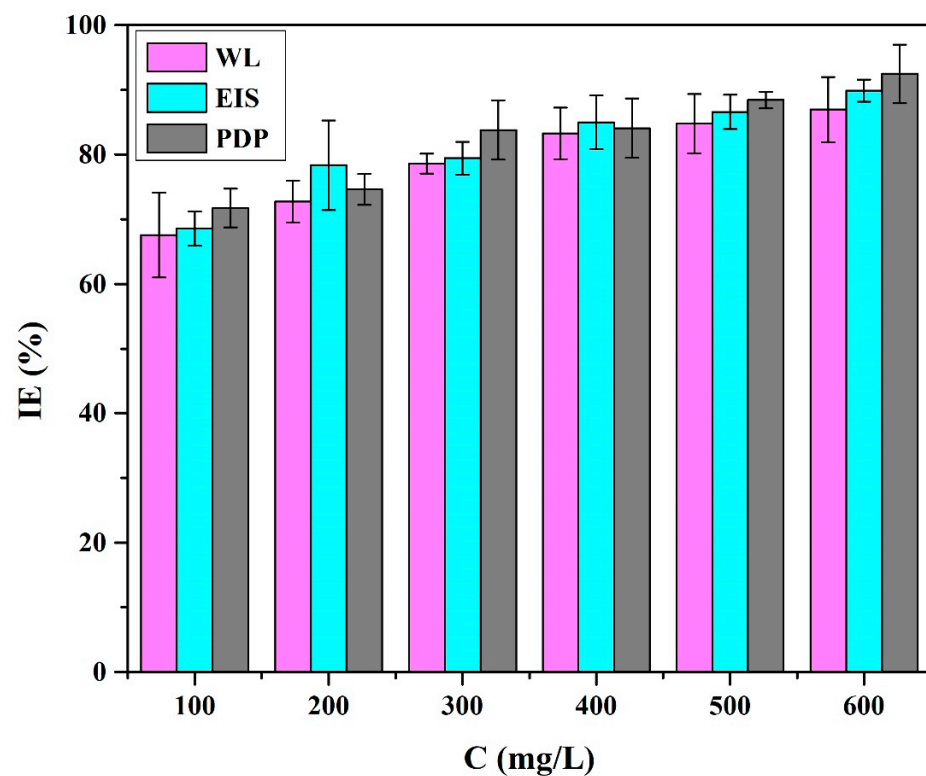


Figure 11. Inhibition efficiencies of *C. microphyllus*-derived film (extract) obtained by different techniques at several inhibitor concentrations.

Table 7. Comparison of inhibition efficiency between previously reported and the current study.

Sr. No.	Inhibitor	Optimum Concentration	Corrosive Media	IE (%)	Ref.
1	<i>Citrullus lanatus</i>	800 ppm	1 M HCl	91	[2]
2	<i>Eucalyptus</i>	800 ppm	1 M HCl	88	[6]
3	Garlic	10 cm ³ /L	0.5 M H ₂ SO ₄	88	[10]
4	<i>Cuscuta reflexa</i>	2 g/L	1 M HCl	81	[27]
5	<i>Glycyrrhiza glabra</i>	800 ppm	1 M HCl	88	[40]
6	<i>Lavandula mairei</i>	0.4 g/L	1 M HCl	92	[43]
7	<i>Lilium brownii</i>	200 mg/L	0.5 M H ₂ SO ₄	85	[44]
8	<i>Achyranthes aspera</i>	500 ppm	0.5 M H ₂ SO ₄	90	[52]
9	<i>Aegle marmelos</i>	500 ppm	0.5 M H ₂ SO ₄	83	[85]
10	<i>Asparagus racemosus</i>	100 mg/L	0.5 M H ₂ SO ₄	93	[86]
11	<i>Myristica fragrans</i>	500 mg/L	0.5 M H ₂ SO ₄	87	[61]
12	<i>Ficus religiosa</i>	500 mg/L	0.5 M H ₂ SO ₄	92	[62]
13	<i>Alkana tinctoria</i>	500 mg/L	0.5 M H ₂ SO ₄	91	[66]
14	<i>Pfaffia paniculate</i>	600 mg/L	0.5 M H ₂ SO ₄	88	[73]
15	<i>Convolvulus microphyllus</i>	600 mg/L	0.5 M H ₂ SO ₄	92	This work

5. Conclusions

The anti-corrosive properties of *C. microphyllus*-derived film (extract) in 0.5 M sulfuric acid were found to be effective for low carbon steel. Based on the results obtained, the following observations can be made:

- ❖ Electrochemical analysis revealed that the inhibitory effect of *C. microphyllus*-derived film (extract) at a concentration of 600 mg/L provides approximately 92% protection against corrosion for low carbon steel at 298 K.
- ❖ Potentiodynamic polarization estimates indicated that this natural product is a mixed-type inhibitor and also functions as an adsorptive inhibitor. Therefore, the efficiency of the inhibition may be improved by increasing the inhibitor concentration.
- ❖ When the concentration of the inhibitor was increased, electrochemical impedance spectroscopy showed a decrease in the electrical double layer's CPE and an increase in the charge transfer resistance.
- ❖ These findings further demonstrate that the *C. microphyllus*-derived film (extract) extract only affects the metal/solution interface by adsorption.
- ❖ The FT-IR technique demonstrated the presence of heteroatoms and unsaturated mixtures that were used as inhibitors.
- ❖ The coordination connections between the inhibitor molecules and Fe²⁺ were confirmed by the UV-visible spectroscopic technique.
- ❖ The SEM the AFM approaches explored the adsorption of the *C. microphyllus*-derived film (extract) inhibitor on a metal substrate.
- ❖ The experimental results indicate that these inhibitor compounds are strongly physisorbed and chemisorbed onto the LCS surface.
- ❖ Studies in DFT, MC, and MDS demonstrated that inhibitors frequently cured and safeguarded metals due to their distinct ability to attract and withdraw electrons from metals.

Author Contributions: Conceptualization, R.H. and R.V.; methodology, O.D.; software, A.B.; validation, R.H. and O.D.; formal analysis, R.H.; investigation, R.H.; resources, S.-C.K.; data curation, R.V.; writing—original draft preparation, R.H.; writing—review and editing, O.D.; visualization, R.H.; supervision, O.D. and S.-C.K.; project administration, S.-C.K.; funding acquisition, S.-C.K. All authors have read and agreed to the published version of the manuscript.

Funding: This research was supported by the NRF (National Research Foundation) of Korea funded by the Basic Science Research Program through the Ministry of Education (2020R1I1A3052258). In addition, this work was also supported by the Technology Development Program (S3060516) funded by the Ministry of SMEs and Startups (MSS, Korea) in 2021.

Institutional Review Board Statement: Not applicable.

Informed Consent Statement: Not applicable.

Data Availability Statement: Data supporting the findings of this study are available within the article.

Conflicts of Interest: The authors declare no conflict of interest.

Abbreviations

AFM	Atomic force microscopy	M1	Kaempferol
ASTM	American society for testing and materials	M2	p-hydroxycinnamic acid
DFT	Density functional theory	MSD	Molecular dynamic simulation
EIS	Electrochemical impedance spectroscopy	OCP	Open circuit potential
FTIR	Fourier transform infrared spectroscopy	PDP	Potentiodynamic polarization
IE	Inhibition efficiency	SEM	Scanning electron microscopy
LCS	Low carbon steel	SCE	Saturated calomel electrode

References

- Verma, D.K.; Kazi, M.; Alqahtani, M.S.; Syed, R.; Berdimurodov, E.; Kaya, S.; Salim, R.; Asatkar, A.; Haldhar, R. N-hydroxybenzothioamide derivatives as green and efficient corrosion inhibitors for mild steel: Experimental, DFT and MC simulation approach. *J. Mol. Struct.* **2021**, *1241*, 130648. [[CrossRef](#)]
- Dehghani, A.; Bahlakeh, G.; Ramezanzadeh, B.; Ramezanzadeh, M. A combined experimental and theoretical study of green corrosion inhibition of mild steel in HCl solution by aqueous Citrullus lanatus fruit (CLF) extract. *J. Mol. Liq.* **2019**, *279*, 603–624. [[CrossRef](#)]
- Majd, M.T.; Asaldoust, S.; Bahlakeh, G.; Ramezanzadeh, B.; Ramezanzadeh, M. Green method of carbon steel effective corrosion mitigation in 1 M HCl medium protected by Primula vulgaris flower aqueous extract via experimental, atomic-level MC/MD simulation and electronic-level DFT theoretical elucidation. *J. Mol. Liq.* **2019**, *284*, 658–674. [[CrossRef](#)]
- Sanaei, Z.; Bahlakeh, G.; Ramezanzadeh, B.; Ramezanzadeh, M. Application of green molecules from Chicory aqueous extract for steel corrosion mitigation against chloride ions attack; the experimental examinations and electronic/atomic level computational studies. *J. Mol. Liq.* **2019**, *290*, 111176. [[CrossRef](#)]
- Tabatabaei majd, M.; Bahlakeh, G.; Dehghani, A.; Ramezanzadeh, B.; Ramezanzadeh, M. A green complex film based on the extract of Persian Echium amoenum and zinc nitrate for mild steel protection in saline solution; Electrochemical and surface explorations besides dynamic simulation. *J. Mol. Liq.* **2019**, *291*, 111281. [[CrossRef](#)]
- Dehghani, A.; Bahlakeh, G.; Ramezanzadeh, B. Green Eucalyptus leaf extract: A potent source of bio-active corrosion inhibitors for mild steel. *Bioelectrochemistry* **2019**, *130*, 107339. [[CrossRef](#)]
- Dehghani, A.; Bahlakeh, G.; Ramezanzadeh, B.; Ramezanzadeh, M. Aloysia citrodora leaves extract corrosion retardation effect on mild-steel in acidic solution: Molecular/atomic scales and electrochemical explorations. *J. Mol. Liq.* **2020**, *310*, 113221. [[CrossRef](#)]
- Ramezanzadeh, M.; Bahlakeh, G.; Ramezanzadeh, B. Green synthesis of reduced graphene oxide nanosheets decorated with zinc-centered metal-organic film for epoxy-ester composite coating reinforcement: DFT-D modeling and experimental explorations. *J. Taiwan Inst. Chem. Eng.* **2020**, *114*, 311–330. [[CrossRef](#)]
- Majd, M.T.; Ramezanzadeh, M.; Bahlakeh, G.; Ramezanzadeh, B. Steel corrosion lowering in front of the saline solution by a nitrogen-rich source of green inhibitors: Detailed surface, electrochemical and computational studies. *Constr. Build. Mater.* **2020**, *254*, 119266. [[CrossRef](#)]
- Asfia, M.P.; Rezaei, M.; Bahlakeh, G. Corrosion prevention of AISI 304 stainless steel in hydrochloric acid medium using garlic extract as a green corrosion inhibitor: Electrochemical and theoretical studies. *J. Mol. Liq.* **2020**, *315*, 113679. [[CrossRef](#)]
- Keramatinia, M.; Ramezanzadeh, M.; Bahlakeh, G.; Ramezanzadeh, B. Synthesis of a multi-functional zinc-centered nitrogen-rich graphene-like thin film from natural sources on the steel surface for achieving superior anti-corrosion properties. *Corros. Sci.* **2021**, *178*, 109077. [[CrossRef](#)]
- Mofidabadi, A.H.J.; Bahlakeh, G.; Ramezanzadeh, B. Anti-corrosion performance of the mild steel substrate treated by a novel nanostructure europium oxide-based conversion coating: Electrochemical and surface studies. *Colloids Surf. A Physicochem. Eng. Asp.* **2021**, *609*, 125689. [[CrossRef](#)]
- Lashgari, S.M.; Bahlakeh, G.; Ramezanzadeh, B. Detailed theoretical DFT computation/molecular simulation and electrochemical explorations of Thymus vulgaris leave extract for effective mild-steel corrosion retardation in HCl solution. *J. Mol. Liq.* **2021**, *335*, 115897. [[CrossRef](#)]
- Haldhar, R.; Prasad, D.; Saxena, A.; Singh, P. Valeriana wallichii root extract as a green & sustainable corrosion inhibitor for mild steel in acidic environments: Experimental and theoretical study. *Mater. Chem. Front.* **2018**, *2*, 1225–1237. [[CrossRef](#)]
- Shahini, M.H.; Ramezanzadeh, M.; Bahlakeh, G.; Ramezanzadeh, B. Superior inhibition action of the Mish Gush (MG) leaves extract toward mild steel corrosion in HCl solution: Theoretical and electrochemical studies. *J. Mol. Liq.* **2021**, *332*, 115876. [[CrossRef](#)]

16. Salmasifar, A.; Edraki, M.; Alibakhshi, E.; Ramezanzadeh, B.; Bahlakeh, G. Theoretical design coupled with experimental study of the effectiveness of the inhibitive molecules based on *Cynara scolymus* L extract toward chloride-induced corrosion of steel. *J. Mol. Liq.* **2021**, *332*, 115742. [[CrossRef](#)]
17. Mostafatabar, A.H.; Bahlakeh, G.; Ramezanzadeh, B.; Dehghani, A.; Ramezanzadeh, M. A comprehensive electronic-scale DFT modeling, atomic-level MC/MD simulation, and electrochemical/surface exploration of active nature-inspired phytochemicals based on *Heracleum persicum* seeds phytoextract for effective retardation of the acidic-induced c. *J. Mol. Liq.* **2021**, *331*, 115764. [[CrossRef](#)]
18. Tehrani, M.E.H.N.; Ghahremani, P.; Ramezanzadeh, M.; Bahlakeh, G.; Ramezanzadeh, B. Theoretical and experimental assessment of a green corrosion inhibitor extracted from *Malva sylvestris*. *J. Environ. Chem. Eng.* **2021**, *9*, 105256. [[CrossRef](#)]
19. Salmasifar, A.; Edraki, M.; Alibakhshi, E.; Ramezanzadeh, B.; Bahlakeh, G. Combined electrochemical/surface investigations and computer modeling of the aquatic Artichoke extract molecules corrosion inhibition properties on the mild steel surface immersed in the acidic medium. *J. Mol. Liq.* **2021**, *327*, 114856. [[CrossRef](#)]
20. Lashgari, S.M.; Yari, H.; Mahdavian, M.; Ramezanzadeh, B.; Bahlakeh, G.; Ramezanzadeh, M. Synthesis of graphene oxide nanosheets decorated by nanoporous zeolite-imidazole (ZIF-67) based metal-organic framework with controlled-release corrosion inhibitor performance: Experimental and detailed DFT-D theoretical explorations. *J. Hazard. Mater.* **2021**, *404*, 124068. [[CrossRef](#)]
21. Wagner, H.; Schwarting, G. Struktur der microphyllinsäure aus dem harz von *Convolvulus microphyllus*. *Phytochemistry* **1977**, *16*, 715–717. [[CrossRef](#)]
22. Koch, G.; Varney, J.; Thompson, N.; Moghissi, O.; Gould, M.; Payer, J. *International Measures of Prevention, Application, and Economics of Corrosion Technologies Study*, 1st ed.; NACE International: Houston, TX, USA, 2016.
23. Dehghani, A.; Bahlakeh, G.; Ramezanzadeh, B.; Mofidabadi, A.H.J. Construction of a high-potency anti-corrosive metal-organic film based on europium (III)-benzimidazole: Theoretical and electrochemical investigations. *Constr. Build. Mater.* **2021**, *269*, 121271. [[CrossRef](#)]
24. Keshmiri, N.; Najmi, P.; Ramezanzadeh, B.; Ramezanzadeh, M.; Bahlakeh, G. Nano-scale P, Zn-codoped reduced-graphene oxide incorporated epoxy composite; synthesis, electronic-level DFT-D modeling, and anti-corrosion properties. *Prog. Org. Coat.* **2021**, *159*, 106416. [[CrossRef](#)]
25. Kumar, S.; Vashisht, H.; Olasunkanmi, L.O.; Bahadur, I.; Verma, H.; Goyal, M.; Singh, G.; Ebenso, E.E. Polyurethane Based Triblock Copolymers as Corrosion Inhibitors for Mild Steel in 0.5 M H₂SO₄. *Ind. Eng. Chem. Res.* **2017**, *56*, 441–456. [[CrossRef](#)]
26. Belghiti, M.; Echihi, S.; Mahsoun, A.; Karzazi, Y.; Aboulmouhajir, A.; Dafali, A.; Bahadur, I. Piperine derivatives as green corrosion inhibitors on iron surface; DFT, Monte Carlo dynamics study and complexation modes. *J. Mol. Liq.* **2018**, *261*, 62–75. [[CrossRef](#)]
27. Verma, D.; Khan, F.; Bahadur, I.; Salman, M.; Quraishi, M.; Verma, C.; Ebenso, E.E. Inhibition performance of Glycine max, *Cuscuta reflexa* and *Spirogyra* extracts for mild steel dissolution in acidic medium: Density functional theory and experimental studies. *Results Phys.* **2018**, *10*, 665–674. [[CrossRef](#)]
28. Goyal, M.; Vashisht, H.; Kumar, S.; Bahadur, I. Anti-corrosion performance of eco-friendly inhibitor (2-aminobenzyl) triphenylphosphonium bromide ionic liquid on mild steel in 0.5M sulfuric acid. *J. Mol. Liq.* **2018**, *261*, 162–173. [[CrossRef](#)]
29. Verma, C.; Ebenso, E.E.; Bahadur, I.; Quraishi, M.A. An overview on plant extracts as environmental sustainable and green corrosion inhibitors for metals and alloys in aggressive corrosive media. *J. Mol. Liq.* **2018**, *266*, 577–590. [[CrossRef](#)]
30. Goyal, M.; Kumar, S.; Verma, C.; Bahadur, I.; Ebenso, E.E.; Lgaz, H.; Chung, I.-M. Interfacial adsorption behavior of quaternary phosphonium based ionic liquids on metal-electrolyte interface: Electrochemical, surface characterization and computational approaches. *J. Mol. Liq.* **2020**, *298*, 111995. [[CrossRef](#)]
31. Goyal, M.; Vashisht, H.; Kumar, A.; Kumar, S.; Bahadur, I.; Benhiba, F.; Zarrouk, A. Isopentyltriphenylphosphonium bromide ionic liquid as a newly effective corrosion inhibitor on metal-electrolyte interface in acidic medium: Experimental, surface morphological (SEM-EDX & AFM) and computational analysis. *J. Mol. Liq.* **2020**, *316*, 113838. [[CrossRef](#)]
32. Sadik, K.; El Hamdani, N.; Hachim, M.E.; Byadi, S.; Bahadur, I.; Aboulmouhajir, A. Towards a theoretical understanding of alkaloid-extract Cytisine derivatives of *Retama monosperma* (L.) Boiss. Seeds, as eco-friendly inhibitor for carbon steel corrosion in acidic 1M HCl solution. *J. Theor. Comput. Chem.* **2020**, *19*, 2050013. [[CrossRef](#)]
33. Goyal, M.; Vashisht, H.; Kumar, S.; Bahadur, I.; Benhiba, F.; Zarrouk, A. Acid corrosion inhibition of ferrous and non-ferrous metal by nature friendly Ethoxycarbonylmethyltriphenylphosphonium Bromide (ECMTPB): Experimental and MD simulation evaluation. *J. Mol. Liq.* **2020**, *315*, 113705. [[CrossRef](#)]
34. Kumar, B.; Vashisht, H.; Goyal, M.; Kumar, A.; Benhiba, F.; Prasad, A.K.; Kumar, S.; Bahadur, I.; Zarrouk, A. Study of adsorption mechanism of chalcone derivatives on mild steel-sulfuric acid interface. *J. Mol. Liq.* **2020**, *318*, 113890. [[CrossRef](#)]
35. Daoudi, W.; El Aatiaoui, A.; Dagdag, O.; Zaidi, K.; Haldhar, R.; Kim, S.C.; Oussaid, A.; Aouinti, A.; Berisha, A.; Benhiba, F.; et al. Anti-corrosion coating formation by a biopolymeric extract of *Artemisia herba-alba* plant: Experimental and theoretical investigations. *Coatings* **2023**, *13*, 611. [[CrossRef](#)]
36. Kashani, F.R.; Rezaei, M. Electrochemical studies and molecular simulations on the use of molybdic acid for stabilization of AISI 304 stainless steel passive film in sulfuric acid medium. *J. Mol. Liq.* **2021**, *344*, 117733. [[CrossRef](#)]
37. Verma, D.K.; Al Fantazi, A.; Verma, C.; Khan, F.; Asatkar, A.; Hussain, C.M.; Ebenso, E.E. Experimental and computational studies on hydroxamic acids as environmental friendly chelating corrosion inhibitors for mild steel in aqueous acidic medium. *J. Mol. Liq.* **2020**, *314*, 113651. [[CrossRef](#)]

38. Kashani, F.R.; Rezaei, M. Improving the localized corrosion resistance of 304 stainless steel in HCl solution by adsorption of molybdate ions: Interaction mechanisms at the interface using molecular dynamics simulation and electrochemical noise analysis. *Colloids Surf. A Physicochem. Eng. Asp.* **2022**, *647*, 129085. [[CrossRef](#)]
39. Verma, D.K.; Aslam, R.; Aslam, J.; Quraishi, M.A.; Ebenso, E.E.; Verma, C. Computational Modeling: Theoretical Predictive Tools for Designing of Potential Organic Corrosion Inhibitors. *J. Mol. Struct.* **2021**, *1236*, 130294. [[CrossRef](#)]
40. Alibakhshi, E.; Ramezanzadeh, M.; Bahlakeh, G.; Ramezanzadeh, B.; Mahdavian, M.; Motamedi, M. Glycyrrhiza glabra leaves extract as a green corrosion inhibitor for mild steel in 1 M hydrochloric acid solution: Experimental, molecular dynamics, Monte Carlo and quantum mechanics study. *J. Mol. Liq.* **2018**, *255*, 185–198. [[CrossRef](#)]
41. Jmiai, A.; Tara, A.; El Issami, S.; Hilali, M.; Jbara, O.; Bazzi, L. A new trend in corrosion protection of copper in acidic medium by using Jujube shell extract as an effective green and environmentally safe corrosion inhibitor: Experimental, quantum chemistry approach and Monte Carlo simulation study. *J. Mol. Liq.* **2021**, *322*, 114509. [[CrossRef](#)]
42. Naseri, E.; Hajisafari, M.; Kosari, A.; Talari, M.; Hosseinpour, S.; Davoodi, A. Inhibitive effect of Clopidogrel as a green corrosion inhibitor for mild steel; statistical modeling and quantum Monte Carlo simulation studies. *J. Mol. Liq.* **2018**, *269*, 193–202. [[CrossRef](#)]
43. Berrissoul, A.; Ouarhach, A.; Benhiba, F.; Romane, A.; Zarrouk, A.; Guenbour, A.; Dikici, B.; Dafali, A. Evaluation of Lavandula mairei extract as green inhibitor for mild steel corrosion in 1 M HCl solution. Experimental and theoretical approach. *J. Mol. Liq.* **2020**, *313*, 113493. [[CrossRef](#)]
44. Zuo, X.; Li, W.; Luo, W.; Zhang, X.; Qiang, Y.; Zhang, J.; Li, H.; Tan, B. Research of Liliium brownii leaves extract as a commendable and green inhibitor for X70 steel corrosion in hydrochloric acid. *J. Mol. Liq.* **2021**, *321*, 114914. [[CrossRef](#)]
45. Abdallah, M.; Altass, H.M.; Al-Gorair, A.S.; Al-Fahemi, J.H.; Jahdaly, B.A.A.L.; Soliman, K.A. Natural nutmeg oil as a green corrosion inhibitor for carbon steel in 1.0 M HCl solution: Chemical, electrochemical, and computational methods. *J. Mol. Liq.* **2021**, *323*, 115036. [[CrossRef](#)]
46. Khadom, A.A.; Kadhim, M.M.; Anae, R.A.; Mahood, H.B.; Mahdi, M.S.; Salman, A.W. Theoretical evaluation of Citrus Aurantium Leaf Extract as green inhibitor for chemical and biological corrosion of mild steel in acidic solution: Statistical, molecular dynamics, Docking, and quantum mechanics study. *J. Mol. Liq.* **2021**, *343*, 116978. [[CrossRef](#)]
47. Dagdag, O.; Safi, Z.; Hamed, O.; Jodeh, S.; Wazzan, N.; Haldhar, R.; Safi, S.K.; Berisha, A.; El Gouri, M. Comparative study of some epoxy polymers based on bisphenolic and aromatic diamines: Synthesis, viscosity, thermal properties computational and statistical approaches. *J. Polym. Res.* **2021**, *28*, 165. [[CrossRef](#)]
48. Dagdag, O.; El Bachiri, A.; Hamed, O.; Haldhar, R.; Verma, C.; Ebenso, E.; El Gouri, M. Dendrimeric Epoxy Resins Based on Hexachlorocyclotriphosphazene as a Reactive Flame Retardant Polymeric Materials: A Review. *J. Inorg. Organomet. Polym. Mater.* **2021**, *31*, 3240–3261. [[CrossRef](#)]
49. El-Aouni, N.; Hsissou, R.; Safi, Z.; About, S.; Benhiba, F.; El Azzaoui, J.; Haldhar, R.; Wazzan, N.; Guo, L.; Erramli, H.; et al. Performance of two new epoxy resins as potential corrosion inhibitors for carbon steel in 1MHCl medium: Combining experimental and computational approaches. *Colloids Surf. A Physicochem. Eng. Asp.* **2021**, *626*, 127066. [[CrossRef](#)]
50. Dagdag, O.; Guo, L.; Safi, Z.; Verma, C.; Ebenso, E.E.; Wazzan, N.; Masroor, S.; Haldhar, R.; Jodeh, S.; El Gouri, M. Epoxy resin and TiO₂ composite as anticorrosive material for carbon steel in 3% NaCl medium: Experimental and computational studies. *J. Mol. Liq.* **2020**, *317*, 114249. [[CrossRef](#)]
51. Erramli, H.; Dagdag, O.; Safi, Z.; Wazzan, N.; Guo, L.; About, S.; Ebenso, E.; Verma, C.; Haldhar, R.; El Gouri, M. Trifunctional epoxy resin as anticorrosive material for carbon steel in 1 M HCl: Experimental and computational studies. *Surf. Interfaces* **2020**, *21*, 100707. [[CrossRef](#)]
52. Saxena, A.; Prasad, D.; Haldhar, R. Investigation of Corrosion Inhibition Effect and Adsorption Activities of Achyranthes aspera Extract for Mild Steel in 0.5 M H₂SO₄. *J. Fail. Anal. Prev.* **2018**, *18*, 957–968. [[CrossRef](#)]
53. Haldhar, R.; Prasad, D.; Bahadur, I.; Dagdag, O.; Kaya, S.; Verma, D.K.; Kim, S.-C. Investigation of plant waste as a renewable biomass source to develop efficient, economical and eco-friendly corrosion inhibitor. *J. Mol. Liq.* **2021**, *335*, 116184. [[CrossRef](#)]
54. Saxena, A.; Prasad, D.; Haldhar, R. Use of Syzygium aromaticum extract as green corrosion inhibitor for mild steel in 0.5M H₂SO₄. *Surf. Rev. Lett.* **2018**, *26*, 1850200. [[CrossRef](#)]
55. Zavidovskiy, I.A.; Streletskiy, O.A.; Nuriahmetov, I.F.; Nishchak, O.Y.; Savchenko, N.F.; Tatarintsev, A.A.; Pavlikov, A.V. Highly selective polyene-polyyne resistive gas sensors: Response tuning by low-energy ion irradiation. *J. Compos. Sci.* **2023**, *7*, 156. [[CrossRef](#)]
56. Tucureanu, V.; Matei, A.; Avram, A.M. FTIR spectroscopy for carbon family study. *Crit. Rev. Anal. Chem.* **2016**, *46*, 502–520. [[CrossRef](#)]
57. Saxena, A.; Prasad, D.; Haldhar, R.; Singh, G.; Kumar, A. Use of Sida cordifolia extract as green corrosion inhibitor for mild steel in 0.5 M H₂SO₄. *J. Environ. Chem. Eng.* **2018**, *6*, 694–700. [[CrossRef](#)]
58. Saxena, A.; Prasad, D.; Haldhar, R. Investigation of corrosion inhibition effect and adsorption activities of Cuscuta reflexa extract for mild steel in 0.5 M H₂SO₄. *Bioelectrochemistry* **2018**, *124*, 156–164. [[CrossRef](#)] [[PubMed](#)]
59. Saxena, A.; Prasad, D.; Haldhar, R.; Singh, G.; Kumar, A. Use of Saraca ashoka extract as green corrosion inhibitor for mild steel in 0.5 M H₂SO₄. *J. Mol. Liq.* **2018**, *258*, 89–97. [[CrossRef](#)]

60. Haldhar, R.; Kim, S.-C.; Prasad, D.; Bedair, M.; Bahadur, I.; Kaya, S.; Dagdag, O.; Guo, L. Papaver somniferum as an efficient corrosion inhibitor for iron alloy in acidic condition: DFT, MC simulation, LCMS and electrochemical studies. *J. Mol. Struct.* **2021**, *1242*, 130822. [[CrossRef](#)]
61. Haldhar, R.; Prasad, D.; Saxena, A. Myristica fragrans extract as an eco-friendly corrosion inhibitor for mild steel in 0.5 M H₂SO₄ solution. *J. Environ. Chem. Eng.* **2018**, *6*, 2290–2301. [[CrossRef](#)]
62. Haldhar, R.; Prasad, D.; Saxena, A.; Kumar, R. Experimental and theoretical studies of Ficus religiosa as green corrosion inhibitor for mild steel in 0.5 M H₂SO₄ solution. *Sustain. Chem. Pharm.* **2018**, *9*, 95–105. [[CrossRef](#)]
63. Haldhar, R.; Prasad, D.; Bhardwaj, N. Extraction and experimental studies of Citrus aurantifolia as an economical and green corrosion inhibitor for mild steel in acidic media. *J. Adhes. Sci. Technol.* **2019**, *33*, 1169–1183. [[CrossRef](#)]
64. Haldhar, R.; Prasad, D.; Saxena, A. Armoracia rusticana as sustainable and eco-friendly corrosion inhibitor for mild steel in 0.5M sulphuric acid: Experimental and theoretical investigations. *J. Environ. Chem. Eng.* **2018**, *6*, 5230–5238. [[CrossRef](#)]
65. Haldhar, R.; Prasad, D.; Bhardwaj, N. Surface Adsorption and Corrosion Resistance Performance of Acacia concinna Pod Extract: An Efficient Inhibitor for Mild Steel in Acidic Environment. *Arab. J. Sci. Eng.* **2020**, *45*, 131–141. [[CrossRef](#)]
66. Haldhar, R.; Prasad, D.; Saxena, A.; Kaur, A. Corrosion resistance of mild steel in 0.5 M H₂SO₄ solution by plant extract of Alkana tinctoria: Experimental and theoretical studies. *Eur. Phys. J. Plus* **2018**, *133*, 356. [[CrossRef](#)]
67. Haldhar, R.; Prasad, D.; Bahadur, I.; Dagdag, O.; Berisha, A. Evaluation of Gloriosa superba seeds extract as corrosion inhibition for low carbon steel in sulfuric acidic medium: A combined experimental and computational studies. *J. Mol. Liq.* **2021**, *323*, 114958. [[CrossRef](#)]
68. Haldhar, R.; Prasad, D.; Mandal, N.; Benhiba, F.; Bahadur, I.; Dagdag, O. Anticorrosive properties of a green and sustainable inhibitor from leaves extract of Cannabis sativa plant: Experimental and theoretical approach. *Colloids Surf. A Physicochem. Eng. Asp.* **2021**, *614*, 126211. [[CrossRef](#)]
69. Haldhar, R.; Prasad, D.; Bhardwaj, N. Experimental and Theoretical Evaluation of Acacia catechu Extract as a Natural, Economical and Effective Corrosion Inhibitor for Mild Steel in an Acidic Environment. *J. Bio-Tribo-Corros.* **2020**, *6*, 76. [[CrossRef](#)]
70. Haldhar, R.; Prasad, D.; Kamboj, D.; Kaya, S.; Dagdag, O.; Guo, L. Corrosion inhibition, surface adsorption and computational studies of Momordica charantia extract: A sustainable and green approach. *SN Appl. Sci.* **2021**, *3*, 25. [[CrossRef](#)]
71. Haldhar, R.; Prasad, D. Corrosion Resistance and Surface Protective Performance of Waste Material of Eucalyptus globulus for Low Carbon Steel. *J. Bio-Tribo-Corros.* **2020**, *6*, 48. [[CrossRef](#)]
72. Saxena, A.; Prasad, D.; Haldhar, R. Withania somnifera extract as green inhibitor for mild steel in 8 % H₂SO₄. *Asian J. Chem.* **2016**, *28*, 2471–2474. [[CrossRef](#)]
73. Haldhar, R.; Prasad, D.; Saharan, H. Performance of Pfaffia paniculata extract towards corrosion mitigation of low-carbon steel in an acidic environment. *Int. J. Ind. Chem.* **2020**, *11*, 1–12. [[CrossRef](#)]
74. Haldhar, R.; Prasad, D.; Nguyen, L.T.; Kaya, S.; Bahadur, I.; Dagdag, O.; Kim, S.-C. Corrosion inhibition, surface adsorption and computational studies of Swertia chirata extract: A sustainable and green approach. *Mater. Chem. Phys.* **2021**, *267*, 124613. [[CrossRef](#)]
75. Benhiba, F.; Hsissou, R.; Benzekri, Z.; Echihi, S.; El-Blilak, J.; Boukhris, S.; Bellaouchou, A.; Guenbour, A.; Oudda, H.; Warad, I.; et al. DFT/electronic scale, MD simulation and evaluation of 6-methyl-2-(p-tolyl)-1,4-dihydroquinoxaline as a potential corrosion inhibition. *J. Mol. Liq.* **2021**, *335*, 116539. [[CrossRef](#)]
76. Dagdag, O.; Safi, Z.; Wazzan, N.; Erramli, H.; Guo, L.; Mkadmh, A.M.; Verma, C.; Ebenso, E.; El Gana, L.; El Harfi, A. Highly functionalized epoxy macromolecule as an anti-corrosive material for carbon steel: Computational (DFT, MDS), surface (SEM-EDS) and electrochemical (OCP, PDP, EIS) studies. *J. Mol. Liq.* **2020**, *302*, 112535. [[CrossRef](#)]
77. Salman, M.; Ansari, K.R.; Srivastava, V.; Chauhan, D.S.; Haque, J.; Quraisi, M.A. Chromeno naphthyridines based heterocyclic compounds as novel acidizing corrosion inhibitors: Experimental, surface and computational study. *J. Mol. Liq.* **2021**, *322*, 114825. [[CrossRef](#)]
78. Kumar, H.; Yadav, V. Highly efficient and eco-friendly acid corrosion inhibitor for mild steel: Experimental and theoretical study. *J. Mol. Liq.* **2021**, *335*, 116220. [[CrossRef](#)]
79. Kumar, H.; Yadav, V.; Anu, Saha, S.K.; Kang, N. Adsorption and inhibition mechanism of efficient and environment friendly corrosion inhibitor for mild steel: Experimental and theoretical study. *J. Mol. Liq.* **2021**, *338*, 116634. [[CrossRef](#)]
80. Kumar, H.; Dhanda, T. Cyclohexylamine an effective corrosion inhibitor for mild steel in 0.1 N H₂SO₄: Experimental and theoretical (molecular dynamics simulation and FMO) study. *J. Mol. Liq.* **2021**, *327*, 114847. [[CrossRef](#)]
81. Mechbal, N.; Belghiti, M.; Benzbiria, N.; Lai, C.-H.; Kaddouri, Y.; Karzazi, Y.; Touzani, R.; Zertoubi, M. Correlation between corrosion inhibition efficiency in sulfuric acid medium and the molecular structures of two newly eco-friendly pyrazole derivatives on iron oxide surface. *J. Mol. Liq.* **2021**, *331*, 115656. [[CrossRef](#)]
82. Liu, Y.; Fan, B.; Xu, B.; Yang, B. Ambient-stable polyethyleneimine functionalized Ti₃C₂T_x nanohybrid corrosion inhibitor for copper in alkaline electrolyte. *Mater. Lett.* **2023**, *337*, 133979. [[CrossRef](#)]
83. Dong, P.; Zhang, Y.; Zhu, S.; Nie, Z.; Ma, H.; Liu, Q.; Li, J. First-Principles Study on the Adsorption Characteristics of Corrosive Species on Passive Film TiO₂ in a NaCl Solution Containing H₂S and CO₂. *Metals* **2022**, *12*, 1160. [[CrossRef](#)]
84. Liu, Z.; Fan, B.; Zhao, J.; Yang, B.; Zheng, X. Benzothiazole derivatives-based supramolecular assemblies as efficient corrosion inhibitors for copper in artificial seawater: Formation, interfacial release and protective mechanisms. *Corros. Science* **2023**, *212*, 110957. [[CrossRef](#)]

85. Bhardwaj, N.; Prasad, D.; Haldhar, R. Study of the Aegle marmelos as a Green Corrosion Inhibitor for Mild Steel in Acidic Medium: Experimental and Theoretical Approach. *J. Bio- Tribo-Corros.* **2018**, *4*, 61. [[CrossRef](#)]
86. Saxena, A.; Prasad, D.; Haldhar, R. Use of Asparagus racemosus extract as green corrosion inhibitor for mild steel in 0.5 M H₂SO₄. *J. Mater. Sci.* **2018**, *53*, 8523–8535. [[CrossRef](#)]

Disclaimer/Publisher's Note: The statements, opinions and data contained in all publications are solely those of the individual author(s) and contributor(s) and not of MDPI and/or the editor(s). MDPI and/or the editor(s) disclaim responsibility for any injury to people or property resulting from any ideas, methods, instructions or products referred to in the content.